Talanta 179 (2018) 569–574

Contents lists available at ScienceDirect

Talanta

journal homepage: www.elsevier.com/locate/talanta

A bio-image sensor for simultaneous detection of multi-neurotransmitters

You-Na Lee*, Koichi Okumura, Tomoko Horio, Tatsuya Iwata, Kazuhiro Takahashi, Toshiaki Hattori, Kazuaki Sawada

Electrical & Electronic Information Eng., Toyohashi University of Technology, Hibarigaoka 1-1, Tempaku-cho, Toyohashi, Aichi 441-8580, Japan

ARTICLE INFO

Keywords:
Simultaneous detection
Bio-image sensor
Enzyme-immobilized membrane
Multi neurotransmitters
Multiplexing bio-image sensor
H^+ diffusion-barrier layer

ABSTRACT

We report here a new bio-image sensor for simultaneous detection of spatial and temporal distribution of multi-neurotransmitters. It consists of multiple enzyme-immobilized membranes on a 128 × 128 pixel array with read-out circuit. Apyrase and acetylcholinesterase (AChE), as selective elements, are used to recognize adenosine 5′-triphosphate (ATP) and acetylcholine (ACh), respectively. To enhance the spatial resolution, hydrogen ion (H^+) diffusion barrier layers are deposited on top of the bio-image sensor and demonstrated their prevention capability. The results are used to design the space among enzyme-immobilized pixels and the null H^+ sensor to minimize the undesired signal overlap by H^+ diffusion. Using this bio-image sensor, we can obtain H^+ diffusion-independent imaging of concentration gradients of ATP and ACh in real-time. The sensing characteristics, such as sensitivity and detection of limit, are determined experimentally. With the proposed bio-image sensor the possibility exists for customizable monitoring of the activities of various neurochemicals by using different kinds of proton-consuming or generating enzymes.

1. Introduction

Chemical neurotransmissions, with which the signaling molecules are called neurotransmitters, are fundamental processes for communication in the nervous system. Recent works have revealed that a single neuron is capable of releasing two or more neurotransmitters [1–3]. The various combinations of co-release neurotransmitters enable neurons to transmit diverse signaling. However, their exact numbers are unknown, and the physiological role has remained poorly understood. Therefore, a spatial and temporal detection of concentration changing by specific molecules in the nervous system can provide clues to neural signaling pathways. In order to acquire this multiplexing information simultaneously, new methods providing the necessary spatiotemporal resolution, particularly being of small enough resolution, are needed.

Both adenosine 5′-triphosphate (ATP) and acetylcholine (ACh) are well-known neurotransmitters that have been identified [4–6]. ATP functions as a cellular energy currency for almost all cellular metabolisms, and as a major cotransmitter together with several other neurotransmitters in the nervous system as well as in glia cells. ACh, the first known neurotransmitter, also acts as a transmitter in the cholinergic system. Corelease involved ATP and ACh from a mammalian motor nerve has been demonstrated, for the first time, using electrophysiological techniques combined with the firefly luciferase assay [7]. While the related functional roles of ATP and ACh have been widely recognized [8], their signaling is still recorded by simple tools, such as a glass microelectrode filled with 2 M KCl, a patch clamp using borosilicate glass and a biosensor consisting of a series of enzyme-based microelectrodes [9–11]. More elaborate tools to analyze simultaneous multifunction of the coreleased ATP and ACh have been expected to provide further insight into their signaling pathway in the nervous system and in other tissues.

Electrochemical techniques for long time recording the spatial concentration gradient of multiple metabolites include scanning electrochemical microscopy (SECM) [12,13], fast-scan cyclic voltammetry (FSCV) [14–17] and integrated-circuit (IC) based microelectrode array (MEA) [18,19]. SECM has been derived from a scanning probe microscopy (SPM) technique using tip electrodes as scanning probes. This method is effective for investigating the spatial distribution and for quantitatively analyzing various materials near the region of steady-state diffusion. But the temporal resolution is limited by the time of one complete scanning pass of all lines in the measuring area. FSCV-based detection, where a triangular wave is applied to electrodes to measure unique cyclic voltammograms, have allowed high selectivity by repetitive redox reaction on the electrode surface at high scan (up to 100 V/s). However, it generates a large background current [20].

Various MEA systems fabricated using a complementary metal oxide semiconductor (CMOS) technology have been proposed to record

* Corresponding author.
E-mail address: lee@ee.tut.ac.jp (Y.-N. Lee).

https://doi.org/10.1016/j.talanta.2017.11.058
Received 4 October 2017; Received in revised form 22 November 2017; Accepted 26 November 2017
Available online 27 November 2017
0039-9140/ © 2017 Elsevier B.V. All rights reserved.

neuronal activities over multiple temporal and spatial scales at subcellular resolution [21]. However, almost all high-density (HD) MEAs have been focused to capture the neuronal phenomena from the electrophysiological activity of neurons [22–25]. Few MEAs for simultaneous detection of different biochemical elements have been demonstrated with low spatial resolution, due to the difficulty of optimizing the potentials applied to each electrode. Miniaturized array size and electrode spacing have been required to capture the activities of co-released neurotransmitters and cell metabolisms on a subcellular level [26].

Previously we have reported ATP and hydrogen ion (H^+) image sensor based on a 128x128 pixel array within an area of 4.774 mm^2 [27]. The frame rate for continuously recording two-dimensional (2D) images at the entire electrode is 30 frames per second by employing a charge-coupled device (CCD) technique. In order to provide multi-detection ability with high selectivity toward ATP and H^+, apyrase coupled with a cross-linkable polymer have been immobilized on the array in the size of 250 μmx250 μm relatively larger than a sensing area of a single pixel. Sensing the changed H^+ concentration is necessary to keep pH homeostasis in physiological alteration during monitoring and to distinguish the produced proton after the enzymatic reaction from the diffused protons at nearby pixels [28,29]. In this study, we propose a new bio-image sensor capable of simultaneous detection and real-time imaging of the variation in the concentration of two kinds of neurotransmitters and H^+ for the first time. Furthermore, this bio-image sensor contains a smaller enzyme-immobilized membrane to enhance spatial resolution and the barrier layers preventing the proton diffusion after enzymatic reaction. Here, the properties of the proposed sensor are confirmed through droplets of various concentrations of ATP, ACh and H^+ being injected into an electrolyte solution prepared on top of the sensor to monitor their changing distribution. To detect other combinations of neurotransmitters, the other enzymes producing or consuming H^+ after an enzymatic reaction can be applied.

2. Experimental section

2.1. Detection of ATP, ACh, and H^+

The bio-image sensor consists of a 128x128 pixel array with a read-out circuit and selective enzyme membranes. The H^+ concentration sensing principle of a pixel is similar to a conventional ion sensitive field-effect transistor (ISFET). In our case, a typical supporting layer structure of a sensing area is displaced by Si_3N_4/SiO_2/p-type silicon substrate, namely an electrolyte/insulator/semiconductor (EIS) capacitive sensor. EIS system measures the potential difference ($\varnothing_c$) between the electrolyte and Si_3N_4 layer as an ion sensitive membrane. Under electrochemical equilibrium, the potential is given by the Nernst equation [30]:

$$\varnothing_c = V_{REF} + \frac{RT}{nF}\ln\alpha_{H^+}, \quad (1)$$

Here V_{REF} is the reference electrode voltage, R the gas constant, T the absolute temperature, n the number of moles of electrons transferred in the reaction and F the Faraday constant. Because α_{H^+} is the H^+ concentration, it can be calculated by the measured $\varnothing_c$ at constant V_{REF} and constant T. Even though the theoretical $\varnothing_c$ of the ISFET using Si_3N_4 film should be 58 mV/pH at 20 °C [31], the potential of the pH sensor array used in this study has shown about 35.8 mV/pH due to its read-out circuit and charge transfer amplification [32]. Fig. 1 shows the cross-sectional view of a single pixel and its potential well corresponding to low and high H^+ concentration. The potential difference $\Delta\varnothing_s$ under the sensing area is directly correlated with the variation of H^+ concentration in the electrolyte. Therefore, an enzymatic reaction generating H^+ as by-products can be detected. Apyrase and acetylcholinesterase (AChE) selectively catalyze the breakdown of ATP and ACh respectively into the smaller molecule and acids, on the following reactions [33,34]:

$$ATP + H_2O \xrightarrow{\text{Apyrase}} 2AMP + 2HPO_4^{2-} + 2H^+ \quad (2)$$

$$ACh + H_2O \xrightarrow{\text{AChE}} Colin + \text{Acetate ion} + H^+ \quad (3)$$

Consequently, the proposed bio-image sensor represents indirectly the ATP or ACh concentration as the $\Delta\varnothing_s$ by detecting the production amount of H^+ caused by the oxidation. The data processing of the $\Delta\varnothing_s$ from all pixels are carried out automatically with a measuring program of a PC and read out into the output voltage and 2D image.

2.2. Preparing enzyme membranes and H^+ diffusion-barrier layers

2.2.1. Enzyme membranes

The preparation of a bio-image sensor with enzyme membranes is based on our previous work [27]. The first step of the procedure for immobilizing enzymes on the top of the array chip is the spin coating of 50 μl of a mixture of AChE (10 U/μl) and a light sensitive material, called cross-linking polymer. After drying at room temperature (approximately 10 min), a photolithography method (USH-500BY1; Ushio Inc., Tokyo, Japan) is used to transfer patterns from a photomask to the deposited mixture layer. Here, the enzyme-immobilized pattern accurately corresponds to the figure of the sensing area of the single pixel. Excepting the exposed region where apyrase is entrapped in their cross-linked polymer matrices, the mixture of the other regions is removed by distilled water. Then, these three processes are repeated one more time to immobilize apyrase (1.6 U/μl).

2.2.2. H^+ diffusion-barrier layer

Porous layers made from the cross-linking polymer are placed on the enzyme-immobilized image sensor. They are done to act as a barrier to delay the immigration of the generated H^+ from the enzyme membrane into the electrolyte solution. Cross-linking polymer is attractive due to the biological stability and porous chemical structure binding [35]. The layer is deposited on the whole sensing area of the bio-image sensor almost in the same way as the enzyme membrane. Only the photomask is excepted in the process. A cycle for depositing 0.3-μm-thick layer can be repeated to regulate the thickness. AChE (EC 3.1.1.7) and apyrase (EC 3.6.1.5) in powder purchased from Sigma-Aldrich Co. (St. Louis, MO, USA) are used. Before mixing with BIOSIRFINE®-AWP as a cross-linking polymer purchased from Toyo Cosei Co. (Tokyo, Japan), they are prepared using Millipore water.

2.2.3. Solutions and methods

The electrolyte is a standard buffer solution contained 135 mM NaCl, 5 mM KCl, 2 mM $CaCl_2$, 1 mM $MgCl_2$, 10 mM D-glucose, 1 mM HEPES-NaOH (pH7.4) and Millipore water. The buffer solution resists a variation in pH and could adjust the osmolality between solution and a cell. The sensing area of the bio-image sensor is covered with 90 μl of the buffer solution. Then, to obtain a homogeneous enzymatic reaction from the entire area, a 10-μl droplet of a targeted element is thoroughly mixed into the buffer solution with a pipette. Three kinds of the targeted elements, such as ATP, ACh, and a mixture of ATP and ACh, are prepared at high concentration (0.1–25 mM). The final concentrations of the 10-fold dilution are 0.01, 0.1, 0.25, 0.5, 0.75, 1, and 2.5 mM. ATP disodium salt *n*-hydrate and acetylcholine chloride, purchased from Wako Pure Chemicals (Osaka, Japan) and Sigma-Aldrich Co., are solved in the water to make ATP, ACh and the mixture of ATP and ACh. KCl saturated Ag/AgCl reference electrode supplied by EC FRONTIER CO., Ltd. is used.

3. Results and discussion

The main point of this study is the immobilization of apyrase and AChE on the H^+ sensitive pixel sensor array for simultaneously monitoring the activities of ATP and ACh. According to the type of an entrapped enzyme, ATP and ACh are selectively catalyzed to degrade their

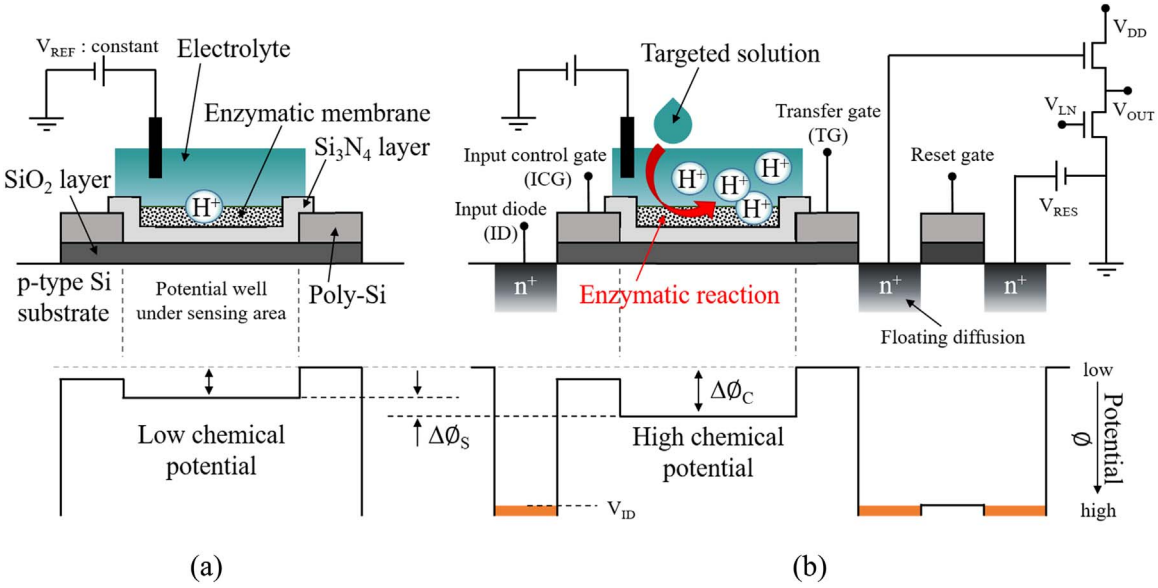

Fig. 1. Schematic representation of the surface potential at an initial state: (a) low hydrogen ion concentration and (b) high hydrogen ion concentration after enzymatic reaction.

by-products and protons. The majority of the generated H^+ is detected electrochemically at the pixels where the enzymatic reaction occurs. In addition, null sensors that have lacked enzymes are monitoring the diffused H^+ through electrolyte or the potential variation of non-specific electrochemical signals during the experiment.

3.1. Diffusion characteristics of H^+ and neurotransmitters

The diffusion of the generated H^+ after the enzymatic reaction in a solution is a very fast (7.62×10^{-5} cm^2/s at room temperature) [36] and unavoidable phenomena in a biological experiment. In order to minimize a signal overlap due to the detection of the diffused H^+ at undesired pixels, we have investigated the phenomena and suggest a

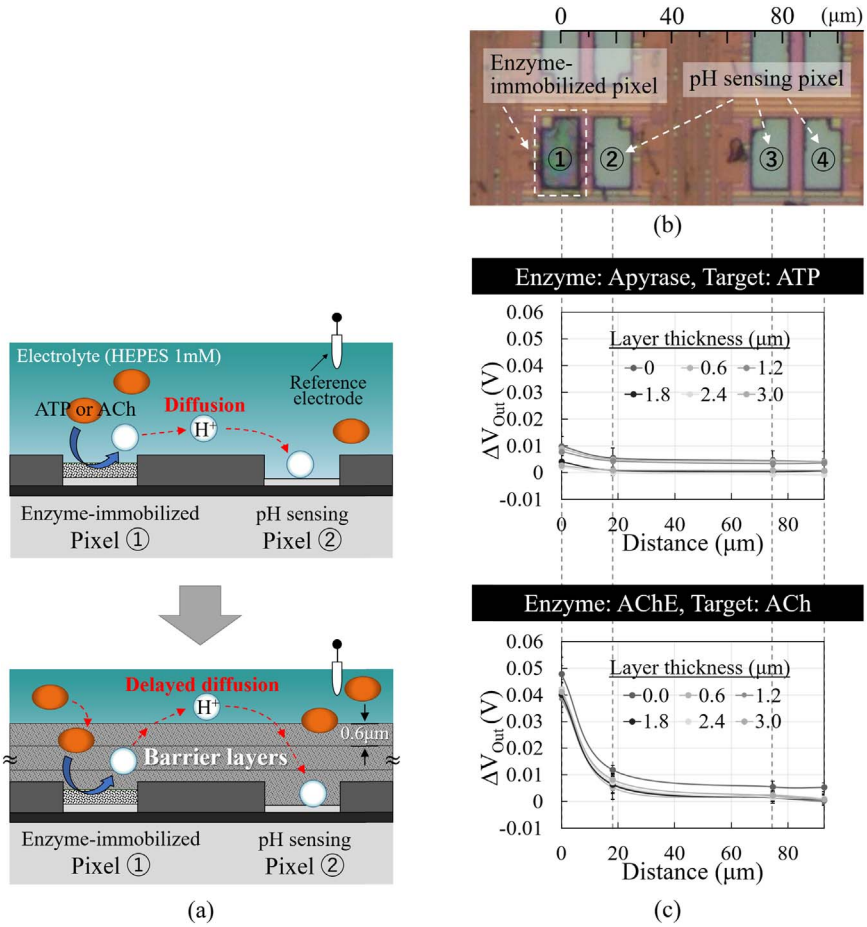

Fig. 2. H^+ diffusion barrier layers. (a) Illustration of the diffusion pathways of the generated H^+ after enzymatic reaction. It immigrates from pixel ① to pixel ② through electrolyte only or electrolyte/porous barrier layers. (b) Optical image of an enzyme-immobilized pixel ① and pH sensing pixel ②, ③, and ④, as null sensors, which are 18.1, 74.6, and 92.7 μm away from the pixel ①, respectively. (c) Diffusion characteristics of the produced and diffused protons according to various barrier layer thicknesses: 0, 0.6, 1.2, 1.8, 2.4, and 3.0 μm. The output voltage represents the response value measured before/after enzymatic reaction between apyrase immobilized at pixel ① and 1 mM ATP (top), or between AChE immobilized at pixel ① and 1 mM ACh (down). It averaged nine groups of the pixel ①, ②, ③, and ④.

barrier layer depositing on the bio-image sensor.

Fig. 2(a) shows the diffusion pathway interrupted by the porous barrier layers which are used to decrease the immigration of the produced H^+ after enzymatic reaction. To demonstrate the H^+ diffusion preventing capabilities of the proposed barrier layer, apyrase or AChE are immobilized only at pixel ① and the surrounding pixels ②, ③, and ④ are used as null sensors to monitor the diffused H^+. Enzyme-immobilized pixels like the pixel ① type are fixed at nine points on an array and placed as far apart as possible from each other to escape the diffusion effect. As shown in Fig. 2(b), pixel ②, ③, and ④ are 18.1, 74.6, and 92.7 μm away from pixel ①, respectively. Diffusion characteristics of the produced and diffused protons after enzymatic reaction are observed according to various barrier layer thicknesses of 0, 0.6, 1.2, 1.8, 2.4, and 3.0 μm. Their response value is provided as the output voltage difference (ΔV_{Out}) between the measured value at 0 s and 170 s after dropping the targeted solution into the electrolyte. In Fig. 2(c), both apyrase-mediated degradation of 1 mM ATP and AChE-mediated degradation of 1 mM ACh shows as the highest signal at the pixel ①. The magnitude of ΔV_{Out} measured at the pixel ②, ③, and ④ are dramatically decreased depending on the distance, because the pixels are detecting the H^+ propagated spherically out from the pixel ①. Furthermore, the decreased ΔV_{Out} according to the layer thickness indicates the consumption of the diffused H^+ from AChE-mediated degradation of 1 mM ACh. In case of the apyrase-mediated degradation of 1 mM ATP, the small output voltage signal makes difficult to distinguish the original signal and the decreased signal by the barrier layer. The diffused H^+ into the layer seems to be chemically bonded with unsatisfied chains of the crosslinking polymer or to be trapped by the porous structure. Because the H^+ detection at the pixel ④ with the barrier layers is nearly not obtained, we design so that the enzyme-immobilized pixels are placed at intervals of over 92.7 μm to minimize signal overlap. To optimize the thickness of the barrier layer, we have to consider a thicker layer can obstruct the inflow of ATP and ACh, as shown in Fig. 3. The saturation speed that indicates the immigration speed of 1 mM ACh from electrolyte to the sensing area surface at the pixel ① is reduced from 36.1 mV/s to 0.1 mV/s, when the barrier layer thickness is changed from 0 μm to 3.0 μm. On the other hand, the saturated value of ΔV_{Out} seems to be independent of the layer thickness. We are considering that most of the unsatisfied chains such as dangling bonds exists on the surface of the barrier layer, and they catch the diffused H^+ as much as the reduced voltage value due to the existence of a barrier layer. Therefore, the thin barrier layer of 0.6 μm has been determined to deposit on the bio-image sensor. When 0.6 μm-thick layer exists on the pixel ①, the saturation speed is 9.8 mV/s with $R^2 = 0.9165$.

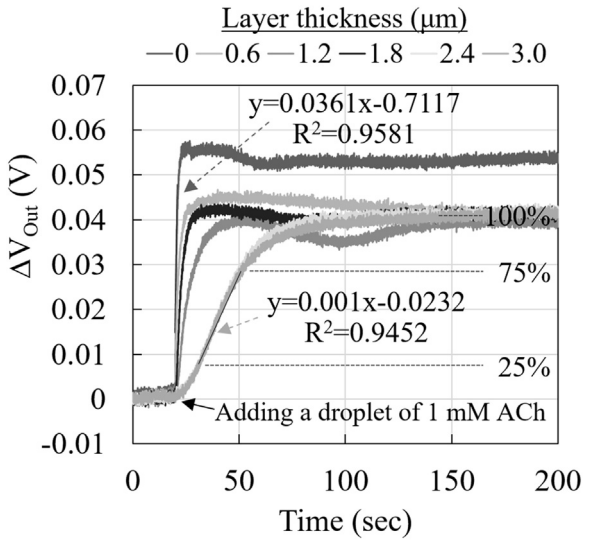

Fig. 3. Saturation speeds according to H^+ barrier layer thickness, when ACh of 1 mM concentration reacts with AChE immobilized at pixel ①.

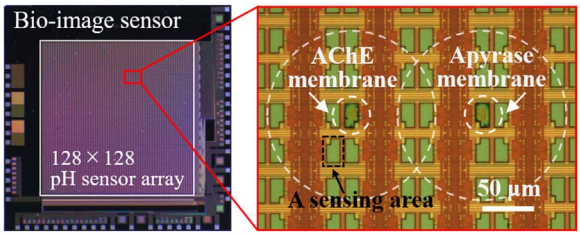

Fig. 4. Optical image of the proposed bio-image sensor with AChE and apyrase immobilized pixels circled. A barrier layer has not deposited yet. The other pixels without enzyme membrane act as pH sensing pixels.

3.2. Bio-image sensor design

The fabricated bio-image sensor before depositing the 0.6 μm-thick barrier layer is shown in Fig. 4. Apyrase-immobilized pixel is located 92.7 μm to ACh-immobilized pixel. A pair of the two kinds of enzyme-immobilized pixels and surrounding null pixels has a space of 280.3 × 223.8 μm^2, thus it is provided as a spatial resolution to distinguish multi-neurotransmitters. 256 pairs are placed to map the activities of ATP, ACh, and H^+ concentration change.

3.3. Imaging of ATP and ACh

Fig. 5 demonstrates the utility of the bio-image sensor to image spatial and temporal distributions of multi-neurotransmitters. As seen in the simultaneous images observed after adding droplets of 1 mM ATP, 1 mM ACh, and 1 mM mixture, the selective detection of ATP and ACh presents as dots by the corresponding enzyme-immobilized pixels. The images at the 0, 5, and 100 s time points provide the spreading movement presented in Fig. 5(a). Here, to examine the effect of the H^+ diffusion barrier layer, we compare the response for a 1 mM mixture solution of ATP and ACh at the horizontally selected pixels from (64,46) to (105,46) in Fig. 5(b). The peaks at 100 s become much more distinguishable than when the barrier layer is absent. The signal intensity of 1 mM ATP, that is approximately 6.2 times smaller than that of 1 mM ACh, could be due to the buffering ability of HEPES in electrolyte or a difference of dissociation constants. Finally, we compare the voltage peaks of the example cross-section extracted from the images of 1 mM ATP, 1 mM ACh, and 1 mM mixture, as shown in Fig. 5(c). ATP and ACh are detected only at apyrase and AChE-immobilized pixels, respectively. It means that enzymes are not mixed during the repeated coating process. Additionally, the overlapping results of the voltage peaks measured individually for detecting ATP and ACh are exactly matched up with the peaks generated by the mixture solution. These results suggest that the detection of multi-neurotransmitters by the proposed bio-image sensor is nearly H^+ diffusion-independent. This hints at that a bio-image sensor can be customizable depending on the kinds of proton-consuming or proton-generating enzymes immobilized on pH image sensor.

3.4. Sensing characteristics

To demonstrate the ATP or ACh sensing capability of our bio-image sensor, the detection characteristics are evaluated as calibration curves determined by averaging 100 pixels each depending on the immobilized enzymes, as shown in Fig. 6. Variability of ΔV_{Out} measured at pixels for a given ATP or ACh concentration increases with increasing concentration. The obtained sensitivities are 55.6 mV/mM for ACh detection with $R^2 = 0.8977$ and 10.9 mV/mM for ATP detection with $R^2 = 0.9539$ in the concentration range up to 0.5 mM. The detection of limits (LODs), calculated from the results by the definition of IUPAC [37], are 0.43 mM ATP at apyrase-immobilized pixel and 0.07 mM ACh

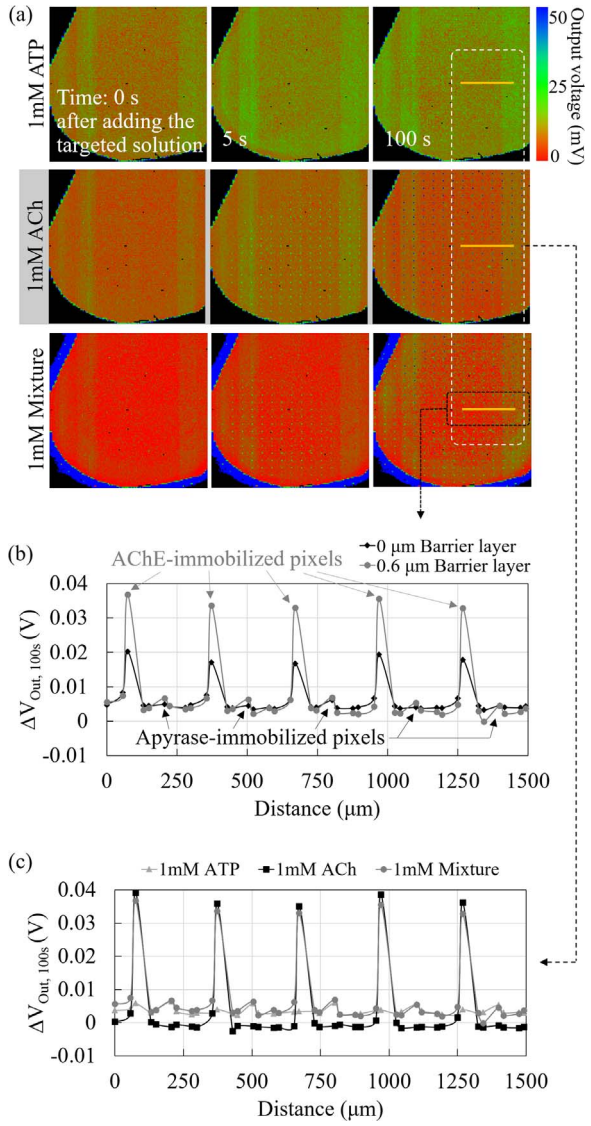

Fig. 5. Simultaneous imaging of ATP, ACh, and their mixture. (a) Simultaneous imaging at 0, 5, and 100 s after adding a droplet of the targeted elements such as 1 mM ATP, 1 mM ACh, and 1 mM mixture. ΔV_{Out} measured by apyrase or AChE-immobilized pixel is proportional to ATP or ACh concentration, respectively. Locations of example cross-sections in **b, c** are from (64,46) to (105,46) by yellow lines. (b) Example cross-section from the image in **a** compared with the measured results without a barrier layer at the same location and detection timing after adding the mixture solution. (c) Example cross-section from the image in **a**.

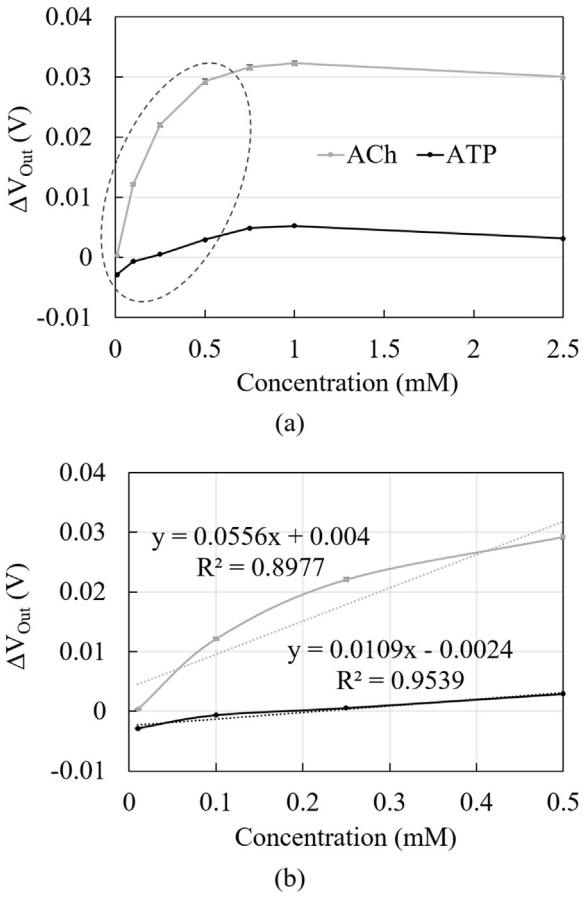

Fig. 6. ATP and ACh sensing characteristics. (a) Calibration curves of the proposed bio-image sensor and (b) linearity in the concentration range up to 0.5 mM of the targeted element. ΔV_{Out} values were determined by averaging 100 pixels each depending on the immobilized enzymes.

at AChE-immobilized pixel, offering enough performance for analyzing their roles in the human cortical or blood [38,39]. A better LOD for sub-μM resolution to analyze the synaptic transmission of neurotransmitters will be pursued in future study. When the bio-image sensor stored at − 4 °C and had been measured 0.5 mM mixture for 10 days to evidence the measurement repeatability, it shows very small output voltage drift of − 0.02 mV/hour at AChE or apyrase-immobilized pixels. It seems to be related the function decline of enzymes.

4. Conclusions

This works shown that a bio-image sensor can simultaneously image the spatial and temporal distribution of multi-neurotransmitters. The porous barrier layers, deposited on top of a H^+ sensitive pixel array with a read-out circuit, provided the enhanced spatial resolution by minimizing signal overlap by H^+ diffusion after enzymatic reaction, as well as most suitable spacing among the enzyme-immobilized pixels and the null pH sensor. Multi-detection ability of the proposed bio-image sensor was demonstrated to obtain simultaneous imaging of the concentration gradients of ATP and ACh in real-time. The sensitivity and detection of limits of ATP and ACh are verified at the corresponding enzyme-immobilized pixels respectively. In order to monitor other combinations of neurotransmitters, we simply need to change the kinds of proton-consuming or-generating enzymes immobilized on a pH image sensor array.

Acknowledgements

This work was supported by JST CREST Grant Number JPMJCR14G2, Japan. This work was partially supported by Adaptable and Seamless Technology Transfer Program from Japan Science and Technology Agency, JST.

References

[1] C.E. Vaaga, M. Borisovska, G.L. Westbrook, Dual-transmitter neurons: functional implications of co-release and co-transmission, Curr. Opin. Neurobiol. 29 (2014) 25–32, http://dx.doi.org/10.1016/j.conb.2014.04.010.

[2] T.S. Hnasko, R.H. Edwards, Neurotransmitter corelease: mechanism and physiological role, Annu. Rev. Physiol. 74 (2012) 225–243, http://dx.doi.org/10.1146/annurev-physiol-020911-153315.

[3] D.J. Barker, D.H. Root, S. Zhang, M. Morales, Multiplexed neurochemical signaling by neurons of the ventral tegmental area, J. Chem. Neuroanat. 73 (2016) 33–42, http://dx.doi.org/10.1016/j.jchemneu.2015.12.016.

[4] H. Zimmermann, ATP and acetylcholine, equal brethren, Neurochem. Int. 52 (2008) 634–648, http://dx.doi.org/10.1016/j.neuint.2007.09.004.

[5] G. Burnstock, Adenosine Triphosphate (ATP), Encycl. Neurosci. 1 (2010) 105–113, http://dx.doi.org/10.1016/B978-008045046-9.00686-0.

[6] M.E. Hasselmo, The role of acetylcholine in learning and memory, Curr. Opin. Neurobiol. 16 (2006) 710–715, http://dx.doi.org/10.1016/j.conb.2006.09.002.
[7] B.E.M. Silinsky, On the association between transmitter secretion and the release of adenine nucleotides from mammalian motor nerve terminals, J. Physiol. 247 (1975) 145–162.
[8] G. Burnstock, The Concept of Cotransmission: focus on ATP as a cotransmitter and its significance in health and disease, Eur. Rev. 22 (2014) 1–17, http://dx.doi.org/10.1017/S1062798713000586.
[9] W. Poelchen, D. Sieler, K. Wirkner, P. Illes, Co-transmitter function of ATP in central catecholaminergic neurons of the rat, Neuroscience 102 (2001) 593–602, http://dx.doi.org/10.1016/S0306-4522(00)00529-7.
[10] N. a. Piskuric, M. Zhang, C. Vollmer, C. a. Nurse, Potential roles of ATP and local neurons in the monitoring of blood O2 content by rat aortic bodies, Exp. Physiol. 99 (2014) 248–261, http://dx.doi.org/10.1113/expphysiol.2013.075408.
[11] R.T.R. Huckstepp, E. Llaudet, A.V. Gourine, CO_2 -Induced ATP-Dependent release of acetylcholine on the ventral surface of the medulla oblongata, PLoS One 11 (2016) e0167861, http://dx.doi.org/10.1371/journal.pone.0167861.
[12] J. Wang, G. Liu, A. Merkoç i, Electrochemical coding technology for simultaneous detection of multiple DNA targets, J. Am. Chem. Soc. 125 (2003) 3214–3215, http://dx.doi.org/10.1021/ja029668z.
[13] K.C. Leonard, A.J. Bard, The study of multireactional electrochemical interfaces via a tip generation/substrate collection mode of scanning electrochemical microscopy: the hydrogen evolution reaction for Mn in acidic solution, J. Am. Chem. Soc. 135 (2013) 15890–15896, http://dx.doi.org/10.1021/ja407395m.
[14] S.K. Smith, C.A. Lee, M.E. Dausch, B.M. Horman, H.B. Patisaul, G.S. McCarty, L.A. Sombers, Simultaneous voltammetric measurements of glucose and dopamine demonstrate the coupling of glucose availability with increased metabolic demand in the rat striatum, ACS Chem. Neurosci. 8 (2017) 272–280, http://dx.doi.org/10.1021/acschemneuro.6b00363.
[15] A. Yakushenko, V. Schöps, D. Mayer, A. Offenhäusser, B. Wolfrum, On-chip fast scan cyclic voltammetry for selective detection of redox active neurotransmitters, Phys. Status Solidi Appl. Mater. Sci. 211 (2014) 1364–1371, http://dx.doi.org/10.1002/pssa.201330276.
[16] J. Dragas, V. Viswam, A. Shadmani, Y. Chen, R. Bounik, A. Stettler, M. Radivojevic, S. Geissler, M.E.J. Obien, J. Muller, A. Hierlemann, In vitro multi-functional microelectrode array featuring 59760 electrodes, 2048 electrophysiology channels, stimulation, impedance measurement, and neurotransmitter detection channels, IEEE J. Solid-State Circuits (2017) 1–15, http://dx.doi.org/10.1109/JSSC.2017.2686580.
[17] E.C. Rama, A. Costa-García, M.T. Fernández-Abedul, Pin-based electrochemical glucose sensor with multiplexing possibilities, Biosens. Bioelectron. 88 (2017) 34–40, http://dx.doi.org/10.1016/j.bios.2016.06.068.
[18] D.L. Bellin, H. Sakhtah, Y. Zhang, A. Price-Whelan, L.E.P. Dietrich, K.L. Shepard, Electrochemical camera chip for simultaneous imaging of multiple metabolites in biofilms, Nat. Commun. 7 (2016) 10535, http://dx.doi.org/10.1038/ncomms10535.
[19] G. Massicotte, S. Carrara, G. Di Micheli, M. Sawan, A CMOS amperometric system for multi-neurotransmitter detection, IEEE Trans. Biomed. Circuits Syst. 10 (2016) 731–741, http://dx.doi.org/10.1109/TBCAS.2015.2490225.
[20] E.S. Bucher, R.M. Wightman, Electrochemical analysis of neurotransmitters, Annu. Rev. Anal. Chem. (Palo Alto. Calif.). 8 (2015) 239–261, http://dx.doi.org/10.1146/annurev-anchem-071114-040426.
[21] M.E.J. Obien, K. Deligkaris, T. Bullmann, D.J. Bakkum, U. Frey, Revealing neuronal function through microelectrode array recordings, Front. Neurosci. 9 (2015) 423, http://dx.doi.org/10.3389/fnins.2014.00423.
[22] R. Liu, R. Chen, A.T. Elthakeb, S.H. Lee, S. Hinckley, M.L. Khraiche, J. Scott, D. Pre, Y. Hwang, A. Tanaka, Y.G. Ro, A.K. Matsushita, X. Dai, C. Soci, S. Biesmans, A. James, J. Nogan, K.L. Jungjohann, D.V. Pete, D.B. Webb, Y. Zou, A.G. Bang, S.A. Dayeh, High density individually addressable nanowire arrays record intracellular activity from primary rodent and human stem cell derived neurons (acs.nanolett.6b04752), Nano Lett. (2017), http://dx.doi.org/10.1021/acs.nanolett.6b04752.
[23] S. Ha, A. Akinin, J. Park, C. Kim, H. Wang, C. Maier, P.P. Mercier, G. Cauwenberghs, Silicon-integrated high-density electrocortical interfaces, Proc. IEEE 105 (2017) 11–33, http://dx.doi.org/10.1109/JPROC.2016.2587690.
[24] M.M. Maharbiz, R. Muller, E. Alon, J.M. Rabaey, J.M. Carmena, Reliable next-generation cortical interfaces for chronic brain-machine interfaces and neuroscience, Proc. IEEE 105 (2017) 73–82, http://dx.doi.org/10.1109/JPROC.2016.2574938.
[25] D. Jäckel, D.J. Bakkum, T.L. Russell, J. Müller, M. Radivojevic, U. Frey, F. Franke, A. Hierlemann, Combination of high-density microelectrode array and patch clamp recordings to enable studies of multisynaptic integration, Sci. Rep. 7 (2017) 978, http://dx.doi.org/10.1038/s41598-017-00981-4.
[26] E. Polo, S. Kruss, Nanosensors for neurotransmitters young investigators in analytical and bioanalytical science, Anal. Bioanal. Chem. 408 (2016) 2727–2741, http://dx.doi.org/10.1007/s00216-015-9160-x.
[27] Y.N. Lee, K. Okumura, T. Iwata, K. Takahashi, T. Hattori, M. Ishida, K. Sawada, Development of an ATP and hydrogen ion image sensor using a patterned apyrase-immobilized membrane, Talanta 161 (2016) 419–424, http://dx.doi.org/10.1016/j.talanta.2016.08.070.
[28] M. Tantama, Y.P. Hung, G. Yellen, Imaging intracellular pH in live cells with a genetically encoded red fluorescent protein sensor, J. Am. Chem. Soc. 133 (2011) 10034–10037, http://dx.doi.org/10.1021/ja202902d.
[29] H.-J. Chung, M.S. Sulkin, J.-S. Kim, C. Goudeseune, H.-Y. Chao, J.W. Song, S.Y. Yang, Y.-Y. Hsu, R. Ghaffari, I.R. Efimov, J.A. Rogers, Stretchable, multiplexed pH sensors with demonstrations on rabbit and human hearts undergoing ischemia, Adv. Healthc. Mater. 3 (2014) 59–68, http://dx.doi.org/10.1002/adhm.201300124.
[30] T. Hizawa, K. Sawada, H. Takao, M. Ishida, Fabrication of a two-dimensional pH image sensor using a charge transfer technique, Sens. Actuators B. Chem. 117 (2006) 509–515, http://dx.doi.org/10.1016/j.snb.2006.01.056.
[31] H. Abe, M. Esashi, T. Matsuo, ISFET's using inorganic gate thin films, IEEE Trans. Electron Devices 26 (1979) 1939–1944, http://dx.doi.org/10.1109/T-ED.1979.19799.
[32] M. Futagawa, D. Suzuki, R. Otake, F. Dasai, M. Ishida, K. Sawada, Fabrication of a 128 × 128 pixels charge transfer type hydrogen ion image sensor, IEEE Trans. Electron Devices 60 (2013) 2634–2639, http://dx.doi.org/10.1109/TED.2013.2268208.
[33] S. Migita, K. Ozasa, T. Tanaka, T. Haruyama, Enzyme-based field-effect transistor for adenosine triphosphate (ATP) sensing, Anal. Sci. 23 (2007) 45–48, http://dx.doi.org/10.2116/analsci.23.45.
[34] S.R. Lee, M.M. Rahman, M. Ishida, K. Sawada, M. Ishida, K. Sawada, Development of a highly-sensitive acetylcholine sensor using a charge-transfer technique on a smart biochip, TrAC Trends Anal. Chem. 28 (2009) 196–203, http://dx.doi.org/10.1016/j.trac.2008.11.009.
[35] A. Sassolas, L.J. Blum, B.D. Leca-Bouvier, Immobilization strategies to develop enzymatic biosensors, Biotechnol. Adv. 30 (2012) 489–511, http://dx.doi.org/10.1016/j.biotechadv.2011.09.003.
[36] S.H. Lee, J.C. Rasaiah, Proton transfer and the mobilities of the H+ and OH- ions from studies of a dissociating model for water, J. Chem. Phys. 135 (2011), http://dx.doi.org/10.1063/1.3632990.
[37] G.L. Long, J.D. Winefordner, Limit of detection a closer look at the IUPAC definition, Anal. Chem. 55 (1983) 712A–724A, http://dx.doi.org/10.1021/ac00258a724.
[38] X.-H. Zhu, H. Qiao, F. Du, Q. Xiong, X. Liu, X. Zhang, K. Ugurbil, W. Chen, Quantitative imaging of energy expenditure in human brain, NeuroImage 60 (2013) 2107–2117, http://dx.doi.org/10.1016/j.neuroimage.2012.02.013.Quantitative.
[39] M. Watanabe, A. Kimura, K. Akasaka, S. Hayashi, Determination of acetylcholine in human blood, Biochem. Med. Metab. Biol. 36 (1986) 355–362, http://dx.doi.org/10.1016/0885-4505(86)90147-7.